Zero-valent Palladium Single-Atoms Catalysts Confined in Black Phosphorus for Efficient Semi-hydrogenation

Cheng Chen[†1,2] , Wei Ou[†3], Kah-Meng Yam[†1,4,11], Shibo Xi[†5], Xiaoxu Zhao[1,6], Si Chen[7], Jing Li[1,11], Pin Lyu[1], Lu Ma[8], Haomin Xu[1], Wei Yu[1], Hanyan Fang[1], Chuanhao Yao[1,9], Xiao Hai,[1,3] Ming Joo Koh[1], Ming Lin[10], Stephen J. Pennycook[4,11], Junling Lu[7], Yonghua Du[8], Chenliang Su[*3], Chun Zhang[*1,4,11], Jiong Lu[*1,11]

[1]Department of Chemistry, National University of Singapore, 3 Science Drive 3, Singapore 117543.

[2]NUS(Suzhou) Research Institute, No. 377 Linquan Street, Suzhou Industrial Park, Suzhou, Jiangsu 215028, China.

[3]SZU-NUS Collaborative Centre and International Collaborative Laboratory of 2D Materials for Optoelectronic Science & Technology, College of Optoelectronic Engineering, Shenzhen University, Shenzhen 518060, China.

[4]Department of Physics, National University of Singapore, 2 Science Drive 3, Singapore 117542.

[5]Institute of Chemical and Engineering Sciences, A*STAR (Agency for Science, Technology and Research), 1 Pesek Road, Jurong Island, Singapore 627833, Singapore.

[6]Department of Materials Science & Engineering, National University of Singapore, 9 Engineering Drive 1, Singapore 117575, Singapore.

[7]Department of Chemical Physics, University of Science and Technology of China, Hefei, 230026, China.

[8]National Synchrotron Light Source II, Brookhaven National Laboratory Upton NY, 11973 USA.

[9]Frontiers Science Center for Flexible Electronics (FSCFE), Shaanxi Institute of Flexible Electronics (SIFE) & Shaanxi Institute of Biomedical Materials and Engineering (SIBME), Northwestern Polytechnical University (NPU), 127 West Youyi Road, Xi'an, 710072, China.

[10]Institute of Materials Research and Engineering, Agency for Science, Technology and Research (A*STAR), 2 Fusionopolis Way, Innovis, #08-03, Singapore 138634, Singapore.

[11]Centre for Advanced 2D Materials and Graphene Research Centre, National University of Singapore, Singapore 117546, Singapore.

†These authors contributed equally to this work.
*Corresponding authors: chmluj@nus.edu.sg, chmsuc@szu.edu.cn, phyzc@nus.edu.sg

Abstract

Single-atom catalysts (SACs) represent a new frontier in heterogeneous catalysis due to their remarkable catalytic properties and maximized atomic utilization. However, single atoms often bond to the support with polarized electron density and thus exhibit a high valence state, limiting their catalytic scopes in many chemical transformations. Here, we demonstrated that two-dimensional (2D) black phosphorus (BP) act as giant phosphorus (P) ligand to confine a high density of single atoms (eg, Pd_1, Pt_1) *via* atomic layer deposition. Unlike other 2D materials, BP with relatively low electronegativity and buckled structure favors the strong confinement of robust zero-valent palladium SACs in the vacancy site. Metallic Pd_1/P SAC shows a highly selective semi-hydrogenation of phenylacetylene towards styrene, outperforming high-valence Pt_1/P SAC, and also distinct from metallic Pd nanoparticles that facilitate the formation of fully hydrogenated products. Our DFT calculations reveal that Pd atom forms covalent-like bonding with adjacent P atoms, wherein H atoms tend to adsorb over electron-rich region for the subsequent

hydrogenation. Zero-valent Pd in the confined space favors a larger energy gain for the synthesis of partially-hydrogenated product over the fully-hydrogenated one. Our work provides a new route towards the synthesis of zero-valent SACs on BP for a wide range of organic transformations.

Introduction

Single atom catalyst (SAC) has drawn an intensive research interest in heterogeneous catalysis because of its unique catalytic properties and maximized atom efficiency [1, 2, 3, 4, 5, 6, 7, 8, 9, 10, 11, 12, 13]. However, the electronic hybridization and polarization between single atoms and support often leads to a high valence state of supported single metal atoms, which significantly limit their catalytic applications in a variety of chemical conversions.[14, 15, 16] Molecular phosphorus ligands with low electronegativity and versatile coordination ability have been widely used to synthesize zero-valent metal-complex compounds as efficient homogenous catalysts for various organic transformations.[17, 18, 19, 20] Inspired by this, we discovered that 2D BP with buckled structure can be viewed as a giant phosphorus ligand to anchor various single-metal atoms with tunable electronic and catalytic properties.[21, 22, 23] Unlike other planar 2D materials such as graphene and-C_3N_4, and MoS_2, the intrinsic coordination properties of phosphorus atoms with a relatively low electronegativity in BP potentially render them as an ideal platform to support low-valence single-metal atoms without additional heteroatom doping. Moreover, the peculiar puckered structure of BP not only provides a cage-like coordination environment to bond single atoms in the confined space but also offers new advantages to enable unique selectivity and activity in catalysis [24].

Here, we demonstrated the rational synthesis of BP supported SACs (eg, Pd_1, Pt_1) with a controllable high loading via the atomic layer deposition (ALD). It is found that Pd atoms are anchored in the divacancy of BP via covalent bonding with the zero-valent state, as confirmed by both experimental and theoretical calculations. In contrast, Pt atoms anchored in the vacancy are prone to bond with two additional oxygen atoms, leading to a high valence state. Zero-valent Pd_1/BP SAC shows an excellent selectivity and activity in the partial hydrogenation of phenylacetylene into styrene, superior to the high-valence Pt_1/BP SAC, and distinct from metallic Pd nanoparticles that promote the formation of fully-hydrogenated products.

Results and discussion

Synthesis of M_1/BP SACs

In contrast to wet-chemical methods, ALD offers a high-precision and controllable synthesis of atomically-dispersed SACs through self-limiting surface reactions.[7, 12, 25] Therefore, we used this technique to fabricate high-loading SACs (M= Pd, Pt) on few-layer BP flakes obtained by electrochemical exfoliation reported in our previous work (refer to supplementing information 1 and Supplementary Figure 1)[26]. Figure 1 illustrates three major steps involved in the synthetic route. Prior to the deposition of metal precursor molecules, exfoliated BP flakes were heated up to150 °C in ALD chamber to remove the possible surface adsorbents. In addition, thermal annealing in this temperature region also facilitate the formation of extra vacancies as the anchor sites as supported by our scanning tunneling microscopy study of bulk BP (Supplementary Figure 2-3).[27, 28] Subsequently, metal organic precursors are deposited and anchored in the vacancy sites of BP flakes to form the metal-phosphorus bonding through the partial removal of organic ligands. Finally, a further ozone (O_3) treatment of these samples allows for the removal

of the remaining ligands of deposited metal precursors to expose the anchored single atoms on BP. In addition, the loading of isolated metal atoms can be precisely tuned by controlling the exposure time to precursors. The maximal loading of SACs can be achieved once all the anchor sites are fully utilized, beyond that the nanoparticles will form (Supplementary Figure 4-6).[29, 30, 31] The maximal loading of Pt_1/BP and Pd_1/BP obtained (the exposure time of 60 seconds) is determined to be 3.7 wt% and 1.5 wt% respectively, based on the standard inductively coupled plasma atomic emission spectrometer (ICP-AES) analysis. When the exposure time further increases to 70 seconds, metal atoms tend to aggregate into nanoparticles (Supplementary Figure 7). It is noted that the maximal loading of metal atoms achieved here is higher than the majority of SACs prepared via ALD in reported literatures[4, 32, 33].

Characterization of M_1/BP SACs

To investigate the morphologies of as-prepared M_1/BP (Pd_1/BP and Pt_1/BP), high-resolution transmission electron microscopy measurements (HRTEM) and state-of-the-art aberration corrected scanning transmission electron microscopy – annular dark field (STEM-ADF) were conducted. To avoid the beam damage of atomically thin BP flakes, 60 kV acceleration voltage was employed in all STEM experiments. Large-field view TEM and STEM images under bright field and dark field modes (Supplementary Figure 8-11) reveal an absence of metal nanoparticles in both Pd_1/BP and Pt_1/BP samples. Instead, we observed a high density of isolated atoms uniformly dispersed on few-layer BP flakes (Figure 2a, 2c, and Supplementary Figure 9,11). Apart from the isolated metal atoms, the observation of BP lattice along the zigzag crystallographic orientations demonstrates that the crystallinity of BP host retains after ALD treatments, consistent with the Raman spectra of as-prepared Pd_1/BP SACs (Supplementary Figure 12). Interestingly, we found that most single metal atoms (both Pd and Pt) are located

exactly at the zigzag lattice of BP with a zone axis [001] rather than randomly dispersed (Figure 2b, 2d). Figure 2e illustrate the corresponding zigzag lattice plane [001] with a lattice distance of 3.3 Å, wherein the solid red circle highlights the possible adsorption site of single metal atoms over the vacancy site of BP along zigzag lattices. This provides one piece of key information to validate the proposed atomic structure of M_1/BP SACs as discussed in a latter section. In addition, the presence of a high density of atomically dispersed metal atoms on BP support is further confirmed by element mapping using energy-dispersive X-ray spectroscopy (Supplementary Figure 13-14). These observations reveal that BP acts a promising 2D support to anchor a high density of single-metal atoms for catalysis.

In order to probe the local structure and valence state of single-metal atoms on BP, we performed X-ray absorption near-edge structure spectroscopy (XANES) and extended X-ray absorption fine structure spectroscopy (EXAFS) measurements of both Pd_1/BP and Pt_1/BP SACs (Figure 3). Figure 3a shows the normalized Pd k-edge XANES spectra of as-prepared Pd_1/BP, Pd foil and PdO as the reference samples. The pre-edge adsorption acquired over Pd_1/BP resembles that of Pd foil, suggesting that Pd atoms in Pd_1/BP adopt a zero-valent state, presumably attributed to the fact that Pd and P have a similar electronegativity[34]. In addition, the white line intensity of Pd_1/BP is much weaker than that PdO, which further confirms its metallic-like valence state of Pd atoms. In contrast, Pt atoms in Pt_1/BP show a high valence state as confirmed by the Pt L3-edge XANES spectroscopic study (Figure 3d). The white line peak of Pt_1/BP is located at 11568.9 eV, close to that of PtO_2 (11569.5 eV) but higher than that of Pt foil (11566 eV). This indicates that Pt in Pt_1/BP exhibits a high oxidation state, although the electronegativity of Pt is similar to that of Pd and P.[33] Such a different behavior between Pt and Pd is ascribed to a high oxidation tendency of Pt precursors introduced by O_3, since the Pt

precursor is unstable and easily oxidized, especially when organic ligands are removed.[4] In order to probe the local structure of both Pd and Pt SACs, we further analyzed the R-space Fourier transform (FT) k^3 EXAFS spectra of these two samples (Figure 3b and 3d). A prominent peak located at 1.7 Å in the spectrum of Pd_1/BP can be assigned to the Pd-P bonds, different from Pd-O and Pd-Pd bonds situated at 1.5 Å (PdO) and 2.5 Å (Pd foil), respectively.[7] By contrast, Pt_1/BP shows a dominant peak around 1.9 Å, different from that of Pt-O bond (1.6 Å) in PtO_2 and Pt-Pt bond (2.6 Å) in Pt foils. Such a feature can be tentatively attributed to the co-existence of Pt-P and Pt-O bonds. The absence of metal-metal bond related features in both EXAFS spectra of Pd_1 and Pt_1 BP suggests the atomic dispersion of metal atoms on BP substrate, in line with the STEM results. In addition, X-ray photoelectron spectroscopy (XPS) results also suggest the presence of metallic-like Pd in Pd_1/BP, while the Pt in Pt_1/BP shows a high oxidation state between +2 to +4 (refer to supplementary information 2 for details). [35, 36]

To further probe the atomic structures of both Pd_1/BP and Pt_1/BP SACs, we preformed the simulation of the XANES spectrum of DFT-relaxed atomic structures in comparison with experimental data. A few structures for both Pd_1/BP and Pt_1/BP were proposed based on atomic lattice imaged STEM, the coordination number and bonding length as determined by the standard spectrum fitting (supplementary information 3). A throughout analysis reveals that Pd atom confined in the DV of BP to form four Pd-P bonds (inset of Figure 3c) shows excellent agreement between experimental XANES data and simulated one. In contrast, the experiment XANES spectrum and simulated one of Pt bonded with four P atoms in DV (supplementary information 3) shows a large discrepancy. Instead, inserting two oxygen atoms into the local coordination structure to form P_2-Pt-O_2-P_2 yields good agreement between simulated and experimental data. These observations further attest the validity of the proposed atomic

structures for both Pd_1 and Pt_1 SACs, consistent with their valence states, and atomic structures imaged by STEM. The zero-valent Pd SACs is expected to facilitate the hydrogeneration reactions for organic transformations.

Selective partial hydrogenation of alkynes to alkenes

The selective hydrogenation of phenylacetylene is of fundamental importance for the styrene production as the footstone of olefin industrial materials.[37] Therefore, we tested the catalytic performance of Pd_1/BP for the selective hydrogenation of various substituted phenylacetylenes (Figure 3g). It turns out that Pd_1/BP exhibits an extremely high conversion and selectivity for ~~the~~ semi-hydrogenation towards the formation of styrene and its derivatives (4 h, 80 °C and 2 bar pressure), outperforming the catalytic activities of Pt_1/BP SACs and Pd nanoparticle counterparts. A number of reactive arene substituents including *para*-bromine and *para*-chlorine groups are tolerated. In addition, similar selectivity and reactivity results were obtained for the aliphatic alkyne substrate. As shown in Figure 3g, Pd_1-BP SAC delivers a conversion of 95%, 100%, 100% and 100% as well as selectivity of 94%, 98%, 93% and 99% for the selective hydrogenation of phenylacetylene to styrene, 4-bromophenylacetylene to 4-bromostyrene, methyl 4-ethynylbenzoate to methyl 4-vinylbenzoate and 3-butynylbenzene to 3-butenylbenzene, respectively. ~~It is noted that Pt_1/BP SACs shows a good selectivity (95%, 95%, 91%, 91% and 87%) in the analogous semi-hydrogenation reactions, which is comparable to Pd_1/BP. However, a higher temperature (100 °C) and pressure (5 bar) are required to achieve a similarly high catalytic conversion of 95%, 95%, 90%, 94% and 95%, as shown in Figure 4c.~~ Therefore, as-prepared Pd_1-BP SAC is superior to Pt_1/BP in the efficient semi-hydrogenation of various substituted phenylacetylenes. The excellent atomic dispersion of Pd atoms in Pd_1/BP results in a high turnover frequency (TOF) of 0.3 s^{-1} in semi-hydrogenation, approximately 60

times higher than that of metal phosphides reported.[38] In addition, Pd nanoparticle on BP, Pd/C, bare BP or Pt_1/BP SACs show either no or poor selectivity (< 5%) for semi-hydrogenation of phenylacetylene to Styrene. It is worth mentioning that the absence of aggregated Pd atoms in Pd_1/BP after the hydrogenation reactions provide support for the high stability of BP-supported SACs (Supplementary Figure 22).

We then performed DFT calculations to probe the underlying mechanism for superior catalytic performance of zero-valent Pd_1/BP in comparison with that of Pt_1/BP for these selective semi-hydrogenation reactions. We first investigated the hydrogen adsorption over both active sites. Incorporation of Pd atoms into the DV induces a noticeable charge redistribution with the four surrounding P atoms, leading to the formation of covalent-like Pd-P bond (Figure 4a). Bader charge analysis revealed that Pd in Pd_1/BP remains a metallic state with an oxidation number close to zero, in excellent agreement with the experimental observation.[39] Furthermore, the calculations show that hydrogen atom tends to adsorb over the electron-rich site as revealed by the charge redistribution plot, i.e. P-Pd bridge site and P atoms. In addition, we also plot the projected density of states (PDOS) of the Pd and the surrounding P atoms bonded to the Pd before and after the H adsorption (Figure 4b and 4c). Before the adsorption, the density of states (DOS) near Fermi level (E_F) has more contribution from the P atoms (indicated by the blue solid line) than Pd atoms (shown by the red solid line). This partially occupied state originated from the covalent bonding interaction between the Pd and the four adjacent P atoms, which also favors the H adsorption. In contrast to Pd_1/BP, Pt_1/BP shows an electron density accumulation close to the highly electronegative O atoms and the two adjacent P atoms (without bonding to O atoms) as viewed in the charge redistribution plot (Figure 4d). PDOS plot of Pt_1/BP reveals a sharp and strong peak contributed by the O atoms near E_F (Figure 4e), much higher than that contributed

by the P atoms. This suggests that the H atoms would preferentially adsorb on the O atoms to form the highly stable hydroxyl OH groups, unfavorable for the subsequent hydrogenation reactions.

To gain a deep understanding of catalytic origin, we then calculated the change of reaction energies for each elementary step associated with this reaction over Pd_1/BP (Figure 4f). To have a direct comparison, we preformed DFT calculations of the relative energy of reactants, intermediates and products involved in both semi-hydrogenation and full hydrogenation of a representative compound, 4-bromophenylacetylene. As shown in Figure 4f, the semi-hydrogenation reaction of 4-bromophenylacetylene over Pd_1/BP shows a larger lowering of the total energy, as compared to the full hydrogenation of 4-bromostyrene into 1-bromo-4-ethylbenzene, leading to the observed selectivity towards the semi-hydrogenated products.

In addition, the higher activity of Pd_1/BP could also arise from a greater ease in the release of the activated H atoms for the hydrogenation reaction. In the case of Pt_1/BP, the O atoms bridged between the P and Pt atoms are prone to capture the H atoms, leading to the formation of highly stable hydroxyl groups. A strong O-H interaction results in a high energy barrier (4.22 eV) for the dissociation of the O-H bond to release the H atoms (Supplementary Figure 23). On the other hand, the zero-valent Pd atom in Pd_1/BP not only favors the adsorption of the H atoms over the electron-rich P-Pd bridge site and P atoms, but also facilitates the H atom release for the subsequent hydrogenation reaction as compared to that of Pt_1/BP.

Conclusions

In summary, we have successfully demonstrated a novel approach for a controllable synthesis of high-density Pd_1 and Pt_1-SACs confined on the surface of BP via ALD process.

Unlike other flat 2D materials, the buckled BP surface acts as a giant phosphorus ligand to confine zero-valent single-metal atoms *via* metal phosphorus interactions. Interestingly, Pd_1/BP with zero-valent state shows a superior conversion (100%) and selectivity (99%) in the selective partial hydrogenation of phenylacetylene and its derivatives to the corresponding styrenes ~~and corresponding substituted styrene~~, and is superior to high-valent Pt_1/BP. The synthesis of zero-valent SACs on BP with peculiar electronic and catalytic properties opens new opportunities for industrially important chemical transformations.

Methods

The characterization of as-prepared catalysts. The metal loadings in all the samples were measured by ICP-AES. XPS measurements were performed using a SPECS system with XR-50 X-ray Mg Ka (1253.7 eV) sources. STEM-ADF imaging was carried out in a Thermo Fisher FEI Titan Themis G2 and an aberration-corrected JEOL ARM-200F system equipped with a cold field emission gun and an ASCOR probe corrector at 60 kV. The images were collected with a half-angle range from ~85 to 280 mrad, and the convergence semiangle was set at ~30 mrad. The imaging dose rate for single frame imaging is estimated as 8×10^5 e/nm$^2 \cdot$s with a total dose of 1.6×10^7 e/nm^2. The dwell time for STEM-ADF image is set as 20 us/pixel. The X-ray absorption near edge structure (XANES) and the extended X-ray absorption fine structure (EXAFS) measurements of Pt L3-edge was carried out at the XAFCA beamline of the Singapore Synchrotron Light Source (SSLS)[59] and the Pd K-edge XAFS data were collected at 7-BM/QAS beamline of the National Synchrotron Light Source II. The storage ring of SSLS operated at 700 MeV with beam current of 250 mA. A Si (111) double-crystal monochromator was applied to

filter the X-ray beam. Pt, and Pd foils were used for the energy calibration, and all samples were measured under transmission mode at room temperature. The EXAFS oscillations χ(k) were extracted and analyzed using the Demeter software package.[40]

XANES simulations. The XANES spectra of Pt K edges of all the structures predicted by DFT were modelled using a finite difference method implemented by FDMNES program.[41] For the FDMNES calculation, the Schrödinger equation is solved with a free shape of potential, which avoids using the muffin-tin approximation and thus better reproduces the theoretical XANES spectrum. For all the calculated XANESs, the final states are calculated inside a sphere with a size of 8 Å. The energy step at the Fermi level is 0.2 eV.

DFT Calculations: All ab initio calculations were done under the spin-polarized Kohn-Sham DFT formalism as implemented in VASP[39, 42], employing the PAW pseudopotentials[43] and a plane wave basis set with a kinetic cut off energy of 400 eV. The PBE format[44] of GGA was adopted for the exchange–correlation functional. The energy and force convergence criteria were set to be 10^{-4} eV and 0.01 eV Å^{-1} respectively for the structural optimizations. For electronic structure calculations, a k-point mesh of 3×3×1 was used to sample the Brillouin zone and the energy convergence criterion was set to be 10^{-5} eV.

Hydrogenation of phenylacetylene and its derivatives. The selective hydrogenation reactions of phenylacetylene and its derivatives were all carried out in an autoclave. 0.5 mmol of substrates, 1.0×10^{-3} mmol of catalysts, 15 ml methanol were mixed in the autoclave. Subsequently, the reaction mixture with Pd$_1$/BP SACs was stirred for 4 hours at 80 °C, 2 bar (H$_2$ atmosphere), while that of Pt$_1$/BP catalysts was stirred for 24 hours at 100 °C, 5 bar (H$_2$

atmosphere). The as-obtained products were analyzed by GC-MS (7820A GC system, 5977 E
inert MSD, Agilent Technologies).

Data availability. The data that support the findings of this study are available from the
corresponding author upon reasonable request.

Author Contributions

J. Lu. and C.C. conceived and designed the project. C.C. synthesized the SACs and prepared the
samples. O.W. performed the activity test supervised by C. S. K-M.Y. performed the theoretical
calculations supervised by XX. S.X., Y.D. and M. L. performed the XAFS measurement and
XANES simulation. X.Z. performed the STEM-ADF characterization. W. Y. performed XPS
characterization. C.C., K.Y., C.Z. and J. Lu. wrote the manuscript. All authors participated in the
discussion of the data and editing the manuscript. ~~including M. K., C. Z etc.~~
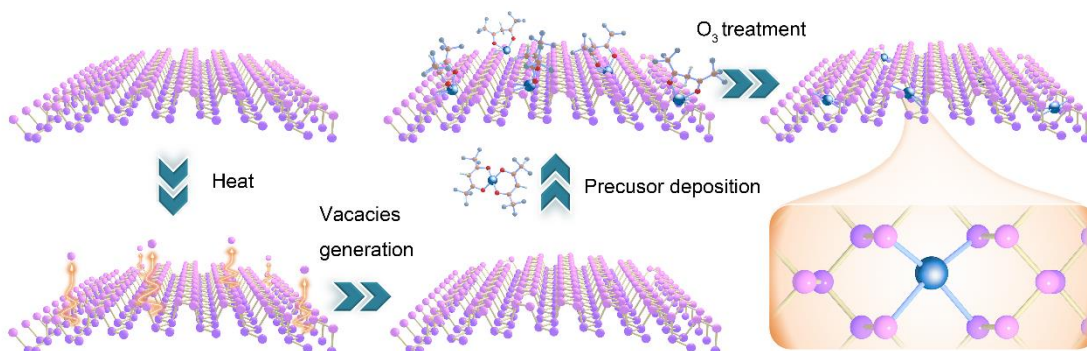
Fig. 1. Schematic illustration of the synthesis of BP confined SACs via ALD. Three major steps involved in the synthetic route: (i) exfoliated few-layer BP flakes were heated up to150 °C in ALD chamber to remove the possible surface adsorbents and to generate extra vacancies as the anchor sites; (ii) Subsequently, metal organic precursors are deposited and anchored in the vacancy sites of BP flakes through the partial removal of organic ligands; (iii) the removal of the remaining ligands of deposited metal precursors via a further ozone (O_3) treatment at 150 °C. Palladium (II) hexafluoroacetylacetonate (Pd(hfac)$_2$) and Trimethyl(methylcyclopentadienyl)-platinum (IV) (MeCpPtMe$_3$) are used as the precursors for the synthesis of Pd$_1$/BP and Pt$_1$/BP, respectively. The balls in pink and purple represent phosphorus in top layer and bottom layer, respectively. The ball in blue represents the metal atom. The balls in red, yellow, and grey represents the oxygen, carbon and hydrogen atoms, respectively.
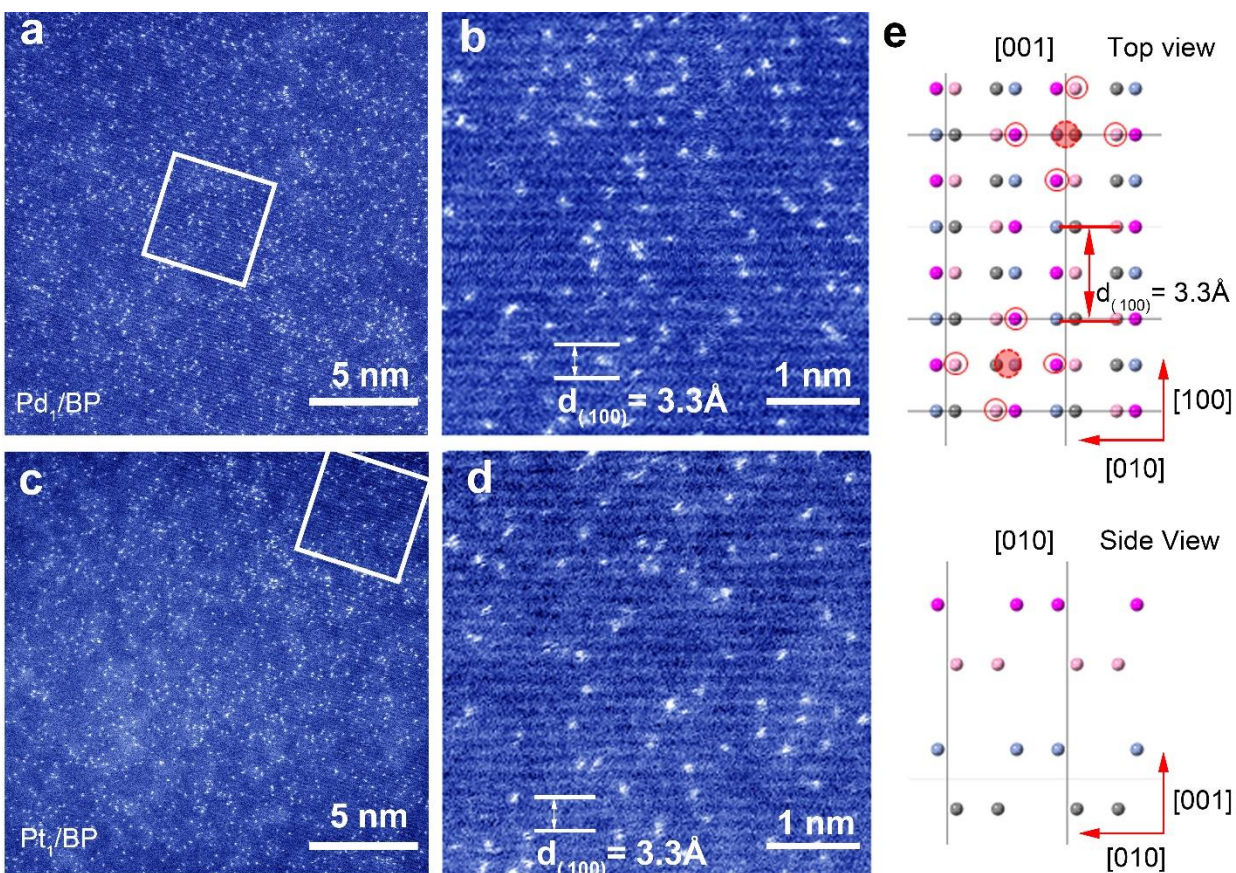
Fig. 2. STEM characterization of Pd₁/BP and Pt₁/BP SACs. Aberration-corrected HAADF-STEM images of Pd$_1$/BP (**a, b**), Pt$_1$/BP (**c, d**); (**e**) The simulated image of M$_1$/BP atomic model corresponding to the zigzag lattice plane of STEM images (**b, d**). The dashed red circle and the four hollow red circles around it highlight the possible adsorption site of single metal atoms over the vacancy site of BP along zigzag lattices and the P atoms connected to the single metal atom. Red, pink, blue and gray balls represent the first, second, third and fourth layer of BP crystal.
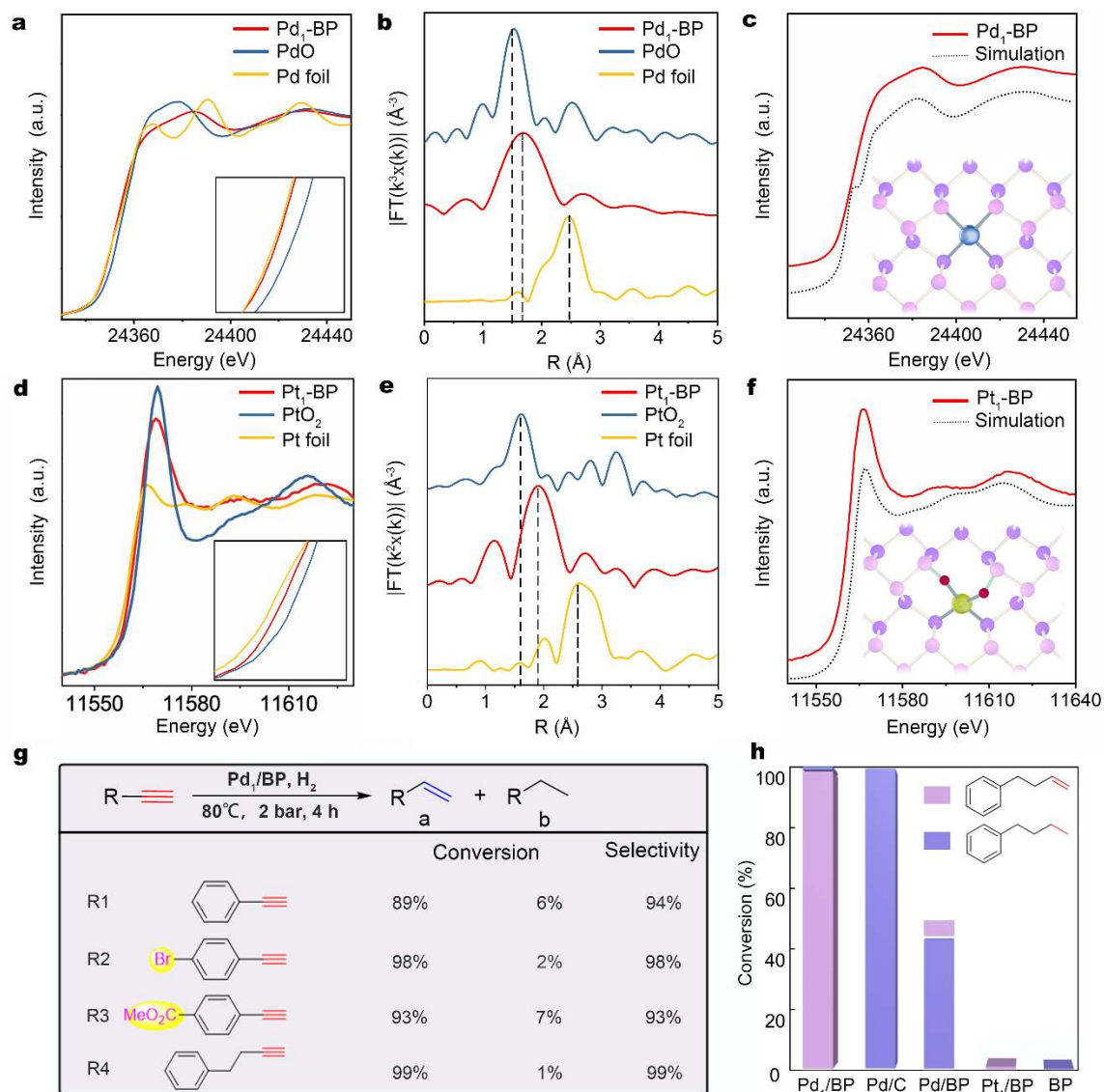
Fig. 3. Local structural characterization of Pd₁/BP and Pt₁/BP SACs via XANES and EXAFS and Catalytic performances of Pd₁/BP SACs. (**a**) Pd K-edge XANES spectrum and (**b**) Fourier transform (FT) EXAFS of Pd₁/BP, PdO, and Pd foil respectively. (**c**) Comparison of the experimental Pd K-edge XANES spectrum of Pd₁/BP (red line) with that of the simulated spectrum (black dot-line) of DFT-modelled structure (inset). (**d**) Pt L3-edge XANES spectrum and (**e**) Fourier transform (FT) EXAFS of Pt₁/BP, PtO₂, and Pt foil respectively. (**f**) Comparison of the experimental Pt L3-edge XANES spectrum of Pt₁/BP (red line) with that of the simulated spectrum (black dot-line) of DFT-modelled structure (inset). (**g**) The catalytic performance (conversion and selectivity) of Pd₁/BP for semi-hydrogenation reactions from phenylacetylene

(R1) to styrene, 4-bromophenylacetylene (R2) to 4-bromostyrene, methyl 4-ethynylbenzoate (R3) to methyl 4-vinylbenzoate and 3-butynylbenzene (R4) to 3-butenylbenzene, respectively. (**h**) The conversion of the partial hydrogenation of 3-butynylbenzene to 3-butenylbenzene using Pd_1/BP SACs in compared to that of commercial Pd/C, Pd nanoparticles on BP (Pd/BP), bare BP nanosheets and Pt_1/BP SACs.
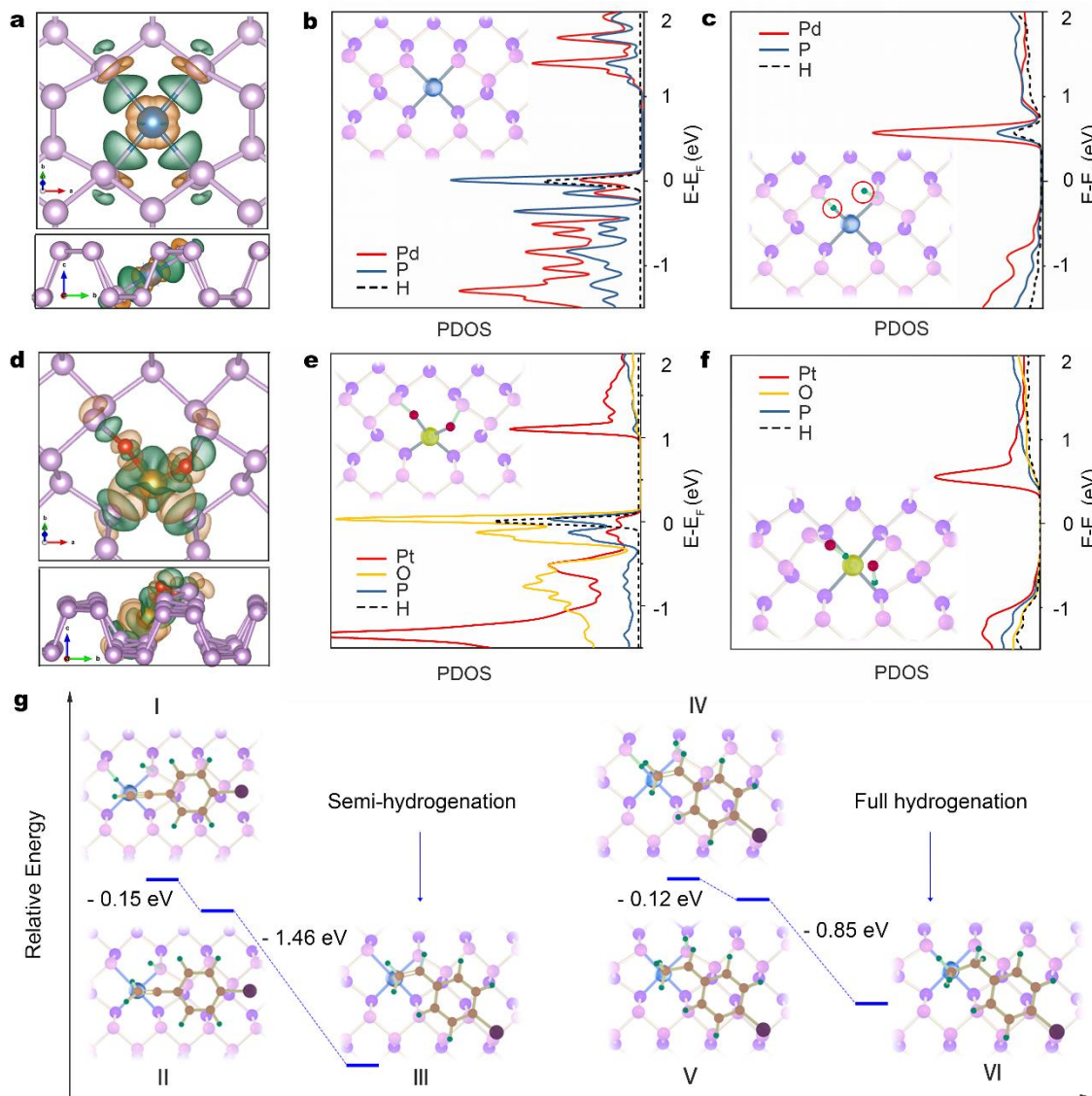

Fig. 4. Investigation of the catalytic origin over BP supported SACs. (**a**) Isosurface of the charge redistribution in Pd_1/BP and (**d**) Pt_1/BP respectively. Note dark green (orange) represents electron accumulation (depletion) region respectively. Projected density of states (PDOS) of Pd_1/BP

(**b**) before and (**c**) after hydrogen adsorption. Inset shows the optimized structure with hydrogen adsorption. Note that the PDOS for the P atoms refers to the two P atoms directly bonded to Pd and subsequently bonded with H. PDOS of Pt_1/BP (**e**) before and (**f**) after hydrogen adsorption. Inset shows the optimized structure with hydrogen adsorption. Note that the PDOS for the P atoms is for the two P atoms directly bonded to the O atoms, which are bonded to the Pt atom. (**g**) The relative energy of the hydrogenation of 4-bromophenylacetylene reactions including reactants, intermediates and products over Pd_1/BP.

References

1.   Qiao B*, et al.* Single-atom catalysis of CO oxidation using Pt 1/FeO x. *Nature chemistry* **3**, 634 (2011).

2.   Yang X-F, Wang A, Qiao B, Li J, Liu J, Zhang T. Single-atom catalysts: a new frontier in heterogeneous catalysis. *Accounts of chemical research* **46**, 1740-1748 (2013).

3.   Lin J*, et al.* Remarkable performance of Ir1/FeO x single-atom catalyst in water gas shift reaction. *Journal of the American Chemical Society* **135**, 15314-15317 (2013).

4.   Sun S*, et al.* Single-atom catalysis using Pt/graphene achieved through atomic layer deposition. *Scientific reports* **3**, 1-9 (2013).

5.   Ding K*, et al.* Identification of active sites in CO oxidation and water-gas shift over supported Pt catalysts. *science* **350**, 189-192 (2015).

6.   Wei H*, et al.* FeO x-supported platinum single-atom and pseudo-single-atom catalysts for chemoselective hydrogenation of functionalized nitroarenes. *Nature communications* **5**, 5634 (2014).

7.   Yan H*, et al.* Single-atom Pd1/graphene catalyst achieved by atomic layer deposition: remarkable performance in selective hydrogenation of 1, 3-butadiene. *Journal of the American Chemical Society* **137**, 10484-10487 (2015).

8.   Wang A, Li J, Zhang T. Heterogeneous single-atom catalysis. *Nature Reviews Chemistry* **2**, 65-81 (2018).

9.   Yang M, Allard LF, Flytzani-Stephanopoulos M. Atomically dispersed Au–(OH) x species bound on titania catalyze the low-temperature water-gas shift reaction. *Journal of the American Chemical Society* **135**, 3768-3771 (2013).

10.   Hai X*, et al.* Engineering Local and Global Structures of Single Co Atoms for a Superior Oxygen Reduction Reaction. *ACS Catalysis* **10**, 5862-5870 (2020).

11.   Zhang H*, et al.* A Graphene‐Supported Single‐Atom FeN5 Catalytic Site for Efficient Electrochemical CO2 Reduction. *Angewandte Chemie* **131**, 15013-15018 (2019).

12.   Yan H*, et al.* Atomic engineering of high-density isolated Co atoms on graphene with proximal-atom controlled reaction selectivity. *Nature communications* **9**, 1-9 (2018).

13.   Lin L*, et al.* A highly CO-tolerant atomically dispersed Pt catalyst for chemoselective hydrogenation. *Nature nanotechnology* **14**, 354-361 (2019).

14.   Cheng N*, et al.* Platinum single-atom and cluster catalysis of the hydrogen evolution reaction. *Nature communications* **7**, 1-9 (2016).

15.   Bakandritsos A*, et al.* Mixed‐Valence Single‐Atom Catalyst Derived from Functionalized Graphene. *Advanced Materials* **31**, 1900323 (2019).

16.   Yang HB*, et al.* Atomically dispersed Ni (I) as the active site for electrochemical CO 2 reduction. *Nature energy* **3**, 140-147 (2018).

17.   Pacchioni G, Bagus PS. Metal-phosphine bonding revisited.. sigma.-Basicity,. pi.-acidity, and the role of phosphorus d orbitals in zerovalent metal-phospine complexes. *Inorganic Chemistry* **31**, 4391-4398 (1992).

18.   Pignolet LM. *Homogeneous catalysis with metal phosphine complexes*. Springer Science & Business Media (2013).

19.   Watanabe H, Kobayashi M, Higuchi K. Reaction of disilanes with acetylenes: I. Stereoselective addition of methoxymethyldisilanes to phenylacetylene catalyzed by group-VIII metal phosphine complexes. *Journal of Organometallic Chemistry* **186**, 51-62 (1980).

20.   Kmentová I, Gotov B, Solcániová E, Toma Š. Study of ligand and base effects on enantioselective allylation catalyzed by Pd (0) phosphine complexes in [bmim][PF 6] ionic liquid. *Green chemistry* **4**, 103-106 (2002).

21.   Tauster S, Fung S, Garten RL. Strong metal-support interactions. Group 8 noble metals supported on titanium dioxide. *Journal of the American Chemical Society* **100**, 170-175 (1978).

22.   van Deelen TW, Mejía CH, de Jong KP. Control of metal-support interactions in heterogeneous catalysts to enhance activity and selectivity. *Nature Catalysis*, 1-16 (2019).

23.   Hu P*, et al.* Electronic metal‐support interactions in single‐atom catalysts. *Angewandte Chemie International Edition* **53**, 3418-3421 (2014).

24.   Morita A. Semiconducting black phosphorus. *Applied Physics A* **39**, 227-242 (1986).

25.   Yan H*, et al.* Bottom-up precise synthesis of stable platinum dimers on graphene. *Nature communications* **8**, 1-11 (2017).

26.   Li J*, et al.* Ultrafast electrochemical expansion of black phosphorus toward high-yield synthesis of few-layer phosphorene. *Chemistry of Materials* **30**, 2742-2749 (2018).

27.   Guo Y, Robertson J. Vacancy and doping states in monolayer and bulk black phosphorus. *Scientific reports* **5**, 1-10 (2015).

28.   Gaberle J, Shluger AL. Structure and properties of intrinsic and extrinsic defects in black phosphorus. *Nanoscale* **10**, 19536-19546 (2018).

29.   Cao L*, et al.* Atomically dispersed iron hydroxide anchored on Pt for preferential oxidation of CO in H 2. *Nature* **565**, 631-635 (2019).

30.   Puurunen RL. Growth per cycle in atomic layer deposition: a theoretical model. *Chemical Vapor Deposition* **9**, 249-257 (2003).

31.   King JS*, et al.* Ultralow loading Pt nanocatalysts prepared by atomic layer deposition on carbon aerogels. *Nano letters* **8**, 2405-2409 (2008).

32.   Ren Y*, et al.* Unraveling the coordination structure-performance relationship in Pt 1/Fe 2 O 3 single-atom catalyst. *Nature communications* **10**, 1-9 (2019).

33. Yan H, *et al.* Bottom-up precise synthesis of stable platinum dimers on graphene. *Nature communications* **8**, 1070 (2017).

34. Boeyens JC. The periodic electronegativity table. *Zeitschrift für Naturforschung B* **63**, 199-209 (2008).

35. Ma Y, Wang H, Li H, Key J, Ji S, Wang R. Synthesis of ultrafine amorphous PtP nanoparticles and the effect of PtP crystallinity on methanol oxidation. *RSC advances* **4**, 20722-20728 (2014).

36. Bai L, *et al.* Black Phosphorus/Platinum Heterostructure: A Highly Efficient Photocatalyst for Solar‐Driven Chemical Reactions. *Advanced Materials* **30**, 1803641 (2018).

37. Fan Q, *et al.* Photodeposited Pd nanoparticles with disordered structure for phenylacetylene semihydrogenation. *Scientific Reports* **7**, 42172 (2017).

38. Chen Y, *et al.* Metal phosphides derived from hydrotalcite precursors toward the selective hydrogenation of phenylacetylene. *ACS Catalysis* **5**, 5756-5765 (2015).

39. Kresse G, Furthmüller J. Efficient iterative schemes for ab initio total-energy calculations using a plane-wave basis set. *Physical review B* **54**, 11169 (1996).

40. Ravel B, Newville M. ATHENA, ARTEMIS, HEPHAESTUS: data analysis for X-ray absorption spectroscopy using IFEFFIT. *Journal of synchrotron radiation* **12**, 537-541 (2005).

41. Bunău O, Joly Y. Self-consistent aspects of x-ray absorption calculations. *Journal of Physics: Condensed Matter* **21**, 345501 (2009).

42. Kresse G, Hafner J. Ab initio molecular dynamics for liquid metals. *Physical Review B* **47**, 558 (1993).

43. Blöchl PE. Projector augmented-wave method. *Physical review B* **50**, 17953 (1994).

44. Perdew JP, Burke K, Ernzerhof M. Generalized gradient approximation made simple. *Physical review letters* **77**, 3865 (1996).